Computer Methods in Biomechanics and Biomedical Engineering

ISSN: 1025-5842 (Print) 1476-8259 (Online) Journal homepage: https://www.tandfonline.com/loi/gcmb20

The effect of hemodynamic parameters in patient-based coronary artery models with serial stenoses: normal and hypertension cases

K. E. Hoque, M. Ferdows, S. Sawall & E. E. Tzirtzilakis

To cite this article: K. E. Hoque, M. Ferdows, S. Sawall & E. E. Tzirtzilakis (2020): The effect of hemodynamic parameters in patient-based coronary artery models with serial stenoses: normal and hypertension cases, Computer Methods in Biomechanics and Biomedical Engineering, DOI: 10.1080/10255842.2020.1737028

To link to this article: https://doi.org/10.1080/10255842.2020.1737028

COMPUTER METHODS IN BIOMECHANICS AND BIOMEDICAL ENGINEERING
https://doi.org/10.1080/10255842.2020.1737028

The effect of hemodynamic parameters in patient-based coronary artery models with serial stenoses: normal and hypertension cases

K. E. Hoque[a,b], M. Ferdows[a], S. Sawall[c] and E. E. Tzirtzilakis[d]

[a]Research group of Fluid Flow Modeling and Simulation, Department of Applied Mathematics, University of Dhaka, Dhaka, Bangladesh; [b]Department of Arts and Sciences, Faculty of Engineering, Ahsanullah University of Science and Technology, Dhaka, Bangladesh; [c]X-Ray Imaging and Computed Tomography, German Cancer Research Center, Heidelberg, Germany; [d]Fluid Dynamics & Turbo-machinery Laboratory, Department of Mechanical Engineering, University of the Peloponnese, Patras, Greece

ABSTRACT

The purpose of this study is to investigate the hemodynamic significance of various degrees of coronary area of stenosis (AS) and multiple sequential stenoses (MSS) in normal and hypertension pressure conditions. MSS in a single branch coronary artery pose challenges to determine the physiological assessment in the prevalent invasive intervention. The hemodynamic parameters of each stenosis are influenced by other stenoses in the single branch of MSS coronary artery. In this study, we entirely use open source tools and techniques for coronary computed tomography angiography (CCTA) image segmentation, 3D reconstruction, grid generation and hemodynamic simulations. The results yield different hemodynamic parameters such as velocity magnitude, mean arterial pressure difference, flow-pressure linear relation, wall shear stress (WSS) and eventually virtual fractional flow reserve (vFFR) allowing for the prediction and the assessment of lumen area severity conditions in MSS coronaries.

ARTICLE HISTORY
Received 7 November 2019
Accepted 27 February 2020

KEYWORDS
CHD; CCTA; vFFR; coronary stenosis; non-invasive

Introduction

Computational Hemodynamics (CHD) parameters play a vital role in assessing the physiological conditions in cardiovascular abnormalities (Cademartiri et al. 2017). Cardiovascular diseases such as atherosclerosis occur due to the result of plaque formation and accumulation of fatty substance inside the vessel wall (Morris et al. 2013). Multiple sequential stenoses (MSS) or coronary aneurysm in a single branch of a coronary artery are responsible for uncertain prognosis of invasive procedures (Bit and Chattopadhay 2018). The hemodynamic significance of each stenosis is influenced by other stenoses emphasizing the importance to evaluate the CHD parameters of each coronary lesion (Ju and Gu 2019). The derived parameters offer the possibility to investigate local atherosclerotic plaque conditions in coronary arteries at a level of detail that is not always accessible with experimental techniques (Kamangar et al. 2017; Seo et al. 2019). Li et al. (2017) demonstrated that there is a linear relationship between flow and pressure in MSS models within idealized coronary models and in in-vitro experiments. They also illustrated that results of simulations of pulsatile and steady are quantitative similar but computational demands highly vary. In this study, we used coronary computed tomography angiography (CCTA) image-based 3D right coronary artery (RCA) models for CHD simulations. The used open source set-up provided us all relevant CHD parameters. In addition, we explored the flow-pressure relation in patient-based 3D models with verified MSS.

It is generally accepted that the atherosclerotic disease occurs in the vicinity of bifurcations and regions with high curvature of arterial walls resulting in obstruction of blood flow in the myocardium (Beier et al. 2016; Bit et al. 2017; Zuin et al. 2019). The presence of coronary obstruction is one of the most important risk factors for an adverse outcome and the coronary revascularization of ischemia-related stenotic coronary lesions can improve patients' functional status in the clinical treatment procedure (Nørgaard et al. 2014). The mechanism of atherosclerotic disease development is quite complex and the hemodynamic factors provide prognostic indicators for individual patients (Bit and Chattopadhay, 2014a; Mittal et al. 2016). The multiple stenoses mechanism in a single branch is more complex than single stenosis in a single branch. There are many researchers who provide

CONTACT M. Ferdows ferdows@du.ac.bd

numerical simulation results within a single stenosis in a single coronary artery branch using a variety of commercial tools. The determination of physiologic conditions in MSS in a single branch of a coronary artery is challenging using interventional procedures. Hence, there is a demand to evaluate CHD parameters in the MSS models using computational procedures.

Currently, invasive Fractional Flow Reserve (FFR) is regarded as the gold standard in the assessment of hemodynamic characteristics for coronary stenosis, and its assessment is recommended prior to coronary revascularization (Shi et al. 2017). However, the high cost and the invasive nature of the procedure may be a drawback (Takagi et al. 2019). In recent years, Coronary Computed Tomography Angiography (CCTA) along with the advanced CHD modeling and simulation results enhancing diagnostic assessment can predict the physiological response of hemodynamic parameters (Nørgaard et al. 2014; Vinoth et al. 2016; Bit et al. 2017). The parameters such as time-average pressure difference, wall shear stress (WSS), pressure-flow relation and eventually virtual Fractional Flow Reserve (vFFR) allow for the prediction and functional assessment of the severity of coronary lesions. The vFFR computations derived from CCTA data represent an alternative method to non-invasively assess hemodynamic parameters in MSS models. Invasive FFR is quite complex and the clinical result is often not satisfactory in case of MSS coronary arteries (Ju and Gu 2019). Numerical simulation of MSS coronary artery flow depends on the downstream pressure that associated with the spacing between the two sequential stenoses (Chen et al. 2016).

Boundary conditions (BCs) are one of the most important parameters to assess the physiological blood flow in simulations (Vignon-Clementel et al. 2006; Bahrami and Norouzi 2018). The effect of BCs are acknowledged for the primary and secondary stenoses (Bit et al. 2020). The explicit lumped parameter BCs are applied for the transient and steady flow simulations. The explicit boundary conditions such as flow and pressure waveforms which mimic the patient's cardiac phases of coronary artery contraction.

In this study, we adopt several techniques for patient-specific 3D model blood flow simulation, such as the CCTA image acquisition, image segmentation, 3D model reconstruction, smooth surface generation on 3D models, grid generation, numerical simulation and result analysis in 3D patient-specific coronary models. The grid independency test was performed for the validation of numerical results simulations. The proximal and distal ratio result of time-average pressure difference produce the vFFR in the single and MSS models. The comparison of vFFR results with some other published results are consistent. The flow-pressure relation provides simulation results in the MSS models are more realistic.

Methodology

CCTA image acquisition and 3D model segmentation

CCTA was performed on a dual-source CT scanner (SOMATOM Force, Siemens Healthineers, Germany). A CCTA dataset was acquired from 67 years old male patient with angina pectoris and severe chest pain by using this dual-source CT scanner in a local hospital (SQUARE Hospital, Dhaka, Bangladesh) as follows:

Coronary CT angiography was performed on a dual-source CT (DSCT) scanner (SOMATOM Force, Siemens Healthineers, Germany). The scanning parameters were as follows: (*i*) tube voltage 100 kV, (*ii*) tube current 450 mAs. Detector collimation $0.75 \times 192 \times 0.6$ mm. Time per gantry revolution 0.25 ms resulting in a temporal resolution of 66 ms. The CTA was performed using prospective ECG-gating. A bolus tracking technique was used for CTA scans and the triggering threshold was set to a CT-value of 100–140 HU in the ascending aorta. The scan was obtained with intravenous injection of 40–60 ml IOHEXOL (350 mg I/mL, IOPAMEDOL 350) at a flow rate of 4–5 ml/s followed by 30 ml saline chaser at the same flow rate. The CTA scan was acquired from 2 cm below the level of the tracheal bifurcation to 1–2 cm below the level of the diaphragm. Image data were routinely automatically reconstructed in best diastolic and best systolic position in the R-R interval with a slice thickness of 0.75 mm, slice increment of 0.75 mm and a medium to smooth convolution kernel B26f. The Field of view (FOV) was 170 mm with a matrix size 256×256.

The baseline characteristics of the target patient are:

Male - Yes, Age - 67 year, BMI - 25.5	Hypertension, Diabetes - Yes
Currently smoking – No	Family history of CAD - No
Percutaneous coronary intervention - No	Previous myocardial infarction – No.

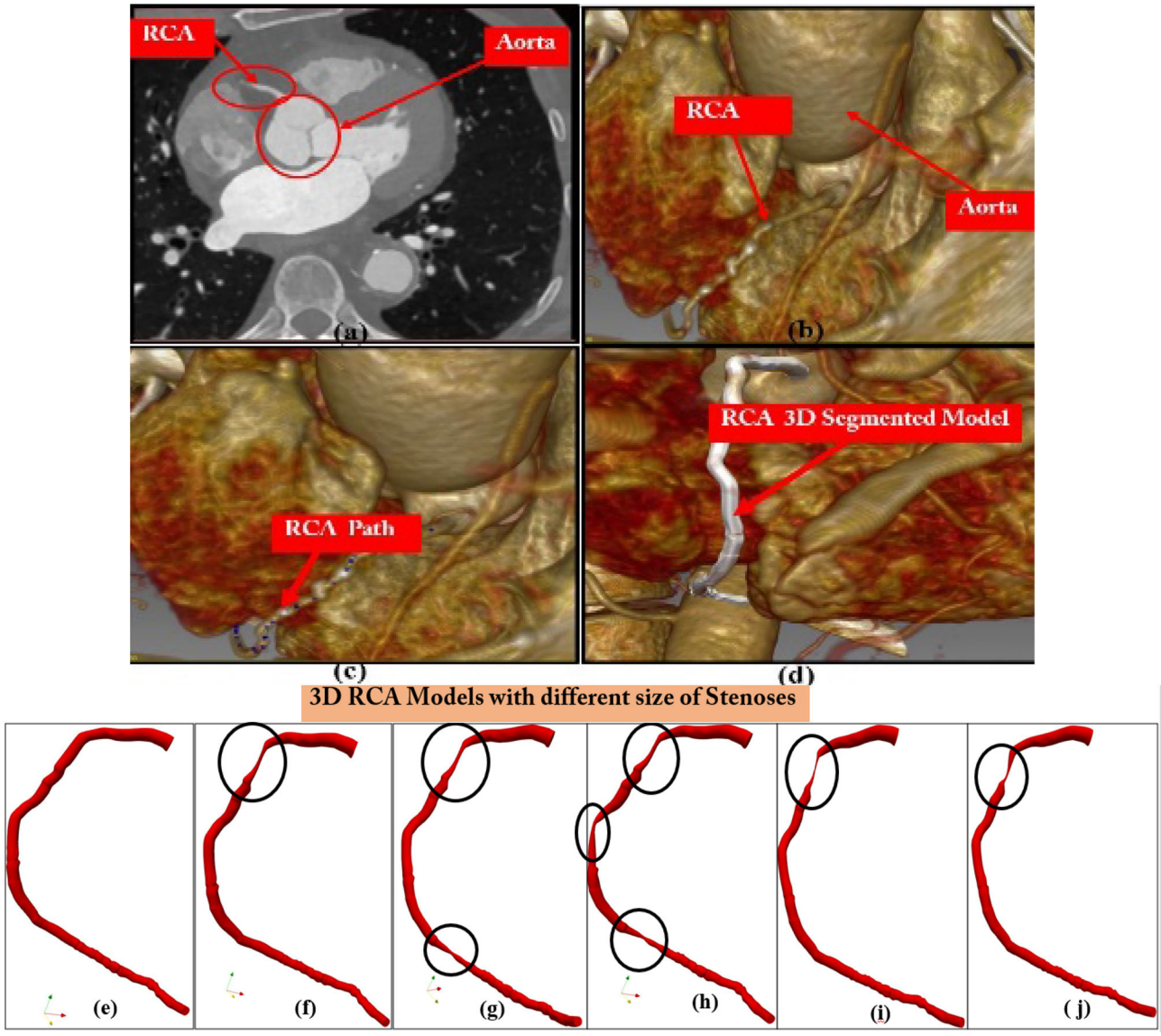

Figure 1. The image (a)–(d) represent the CCTA image slice with the aorta, RCA, rendering view, model path and surface generation from the routine CCTA data. 3D RCA models (e)–(j) show the health and manually created various sizes stenosis/multi-stenosis models.

We applied open source tools (Updegrove et al. 2017) for the CCTA data segmentation, smooth surface generation, 3D patient models' reconstruction and eventually hemodynamic simulations. The simulation results were analyzed using Paraview (Ahrens et al. 2005).

At the beginning of the study, the CCTA image data in DICOM format was imported in the main workbench which is shown in Figure 1(a). The anatomical view is represented in Figure 1(b) by using the volume rendering technique. The rendering view provides concrete hints as to how generate a model path by using the subdivision spacing-based algorithm. The subdivision spacing gave an opportunity to impose some control points along the model path. The control points were combined with the path points to create a 3D model path. For the model path generation, this study follows the volume rendering for certain CT-values (e.g. 100 HU) which is represented in Figure 1(c). The automatic level set algorithm was used with manual 2D ellipse and spline polygon contours for the CCTA image segmentation.

The control points of the path produced an opportunity to segment the CCTA image data. The control points combined with contour points provided a 2D contour along the model path. The lofting technique produced a surface based on NURBS of the segmented 2D contours. Finally, the 3D model surface generated along the path and lofting surface of the

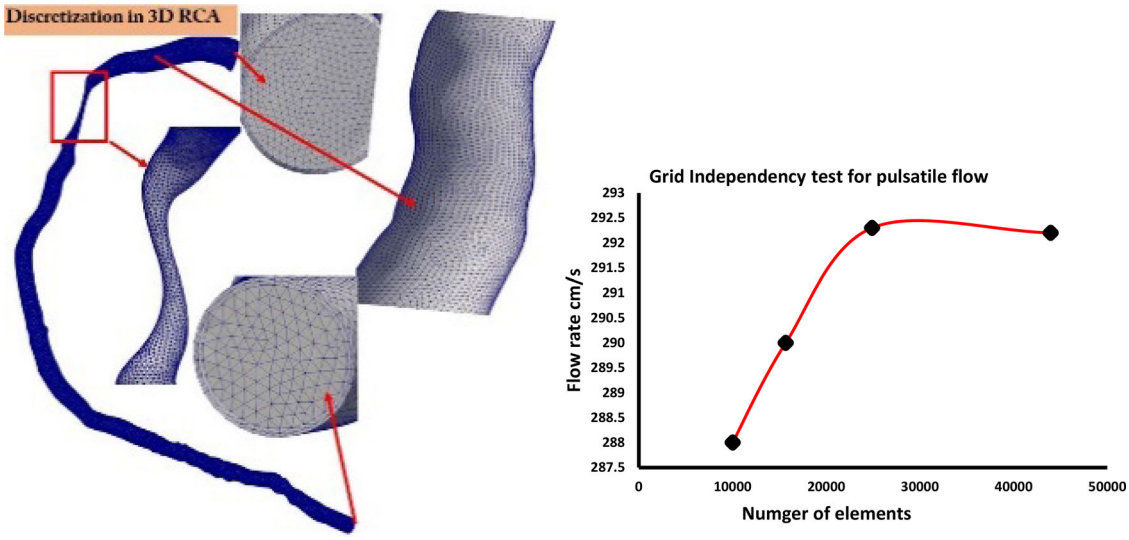

Figure 2. Discretization in the 3D RCA computation domain. The enlarged views show the inlet, outlet, bending and stenosis regions. Grid independency test results in four different densities of grids (very coarse, coarser, coarse and fine) were performed.

patient model is shown in Figure 1(d). It is obvious that the 3D RCA model varies considerably in geometry. This is caused by different radii and tapering in different locations of the RCA. In summary, Figure 1(a–d) illustrates a pipeline from importing CCTA image DICOM data to 3D model segmentation for numerical simulation.

The Right Coronary Artery (RCA) model with different sizes of stenosis are generated by using semi-automatic segmentation, 3D reconstruction and simulation which are performed by the numerical simulation solver (Updegrove et al. 2017). In this study, one patient image dataset with six cases (healthy, one stenosis and multiple stenoses cases) were studied. The impact of hemodynamic assessment is important in single branch coronary main artery with the MSS. The accurate 3D patient-specific model segmentation and reconstruction is a challenging task for numerical blood flow simulation. For 3D model reconstruction, the 2D segmented contours with the lofted surface were imported in the model interface. Now, the polydata approach is used for 3D RCA model reconstruction. The numerical solver is able to connect all 2D segmentation contours to generate a solid RCA model. The area of stenosis (AS) is calculated from as follows (Gottsauner-Wolf et al. 1996):

$$\text{percentage of AS} = \left[1 - \left(\frac{D_{\text{stenosis}}}{D_{\text{normal}}}\right)\right] \times 100\%.$$

Here D_{stenosis} and D_{normal} indicate the diameter of stenosis and healthy areas, respectively. Figure 1(e) represents the healthy RCA model. One concentric stenosis, Figure 1(f), set up near the ostium and the first bending region with 70% stenosis. It is generally accepted that the bifurcation and bending regions are very vulnerable for the formation of atherosclerotic plaques (Hoque et al. 2018). Figure 1(g,h) show the multiple stenoses models. The stenoses location is chosen in a bended region distal from ostium.

The second stenosis is distal the ostium and is also concentric but third stenosis is considered as nearly eccentric. It is generally clinically accepted that the concentric and eccentric stenoses are frequently found in the coronary main branches. Walle et al. (Waller 1989) mentioned that 73% of all atherosclerotic plaques result in an eccentric and 27% in concentric stenosis. Figure 1(i,j) represent the single stenosis models of the RCA main branch with 90% and 80% AS, respectively. Therefore, Figure 1(f,i,j) show the three different sizes such as 70%, 80% and 90% stenosis models, respectively. The AS of lumen area severity reflects the numerical simulation results. The simulation results are providing a proportional relation with the non-invasive assessment of vFFR values and patients' model AS severity.

Numerical methods

A set of assumptions are imposed for the numerical blood flow simulation in the 3D RCA patient-based models. The simulations are derived by solving a large number of highly non-linear partial differential equations. The blood was considered as a Newtonian fluid and incompressible flow, as widely accepted for blood in large vessels (Johnston et al. 2004), with the following fixed values of density, ρ, as 1060 kg/m^3 and dynamic viscosity, μ, as 0.004 Pa·s (Kim et al. 2010; Yoshikawa et al. 2019). The simulation derived by

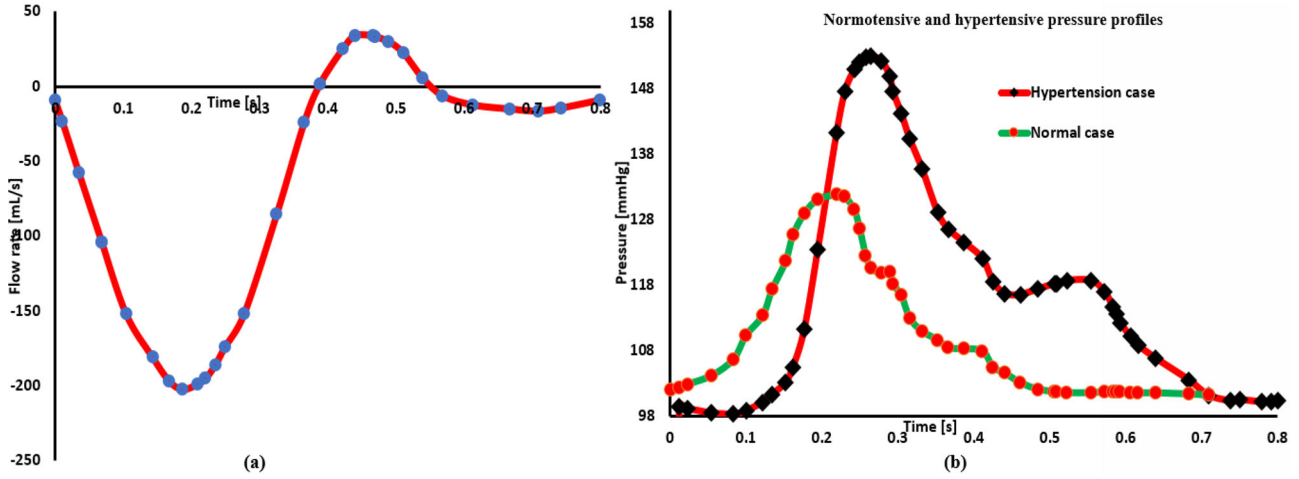

Figure 3. Inlet velocity and outlet pressure profiles are injected in RCA models for CHD simulations. The profiles mimic the pulsatile behavior of inlet and outlet conditions.

solving the conservation of momentum along with the conservation of mass equations, i.e. the three-dimensional Navier-Stokes equations

$$\rho\frac{\partial \mathrm{u}}{\partial t}+\rho(\mathrm{u}.\nabla)\mathrm{u}+\nabla \mathrm{P}=\mu\nabla^2\mathrm{u},\quad \nabla.\mathrm{u}=0, \tag{1}$$

where in u, P, ρ and μ are the velocity, pressure, density and dynamic viscosity of the blood, respectively. To solve the highly non-linear equations, we implied a set of BCs such as no-slip for blood vessel walls as well as Newtonian and incompressible fluid with Neumann types BCs. The inlet fluid flow and outlet pressure (normal and hypertension) waveforms used for the RCA models for CHD simulations are depicted in Figure 2.

The WSS is given by the Stokes relation

$$\tau=\mu[\nabla \mathrm{u}+(\nabla \mathrm{u})^T]+\left(\frac{2}{3}\mu-\kappa\right)(\nabla.\mathrm{u})I, \tag{2}$$

where in∇u, I and κ are the gradient vector, identity vector and dilatational viscosity, respectively. Lumped parameters are implied for controlling the total outflow of distal micro vascular resistance. The mesh, a non-structural mesh with tetrahedral elements of the 3D geometries was generated by using the finite element approach. The mesh independency test was performed for the different densities of the meshes (Figure 3) for the velocity magnitude measurement. The steady and pulsatile flow mesh independency test results indicated that the standard of the coarse and fine meshes were appropriate for numerical simulations.

Finally, vFFR is defined as vFFR $=\frac{\mathrm{P_d}-\mathrm{P_v}}{\mathrm{P_p}-\mathrm{P_v}}$, where $\mathrm{P_p}$ and $\mathrm{P_d}$ are time-averaged proximal and distal stenotic pressure and $\mathrm{P_v}$ is venous pressure considered zero in [Pa] (Pijls et al. 2000; Morris et al. 2018).

Figure 2 represents the inlet flow profile and outlet pressure waveforms. Since the human heartbeat is approximately periodic, one is safe to assume that the blood pressure and flow rate are periodic in time T which is the period of one heartbeat and T = 0.8 s in this case. The spatial boundary conditions of a large arterial tree include one boundary condition at the inlet and one boundary condition at outlet.

The specific inlet and outflow boundary conditions used in this work are shown in Figure 2(a,b) respectively. Figure 2(b) shows two outlet normal and hypertension pressure boundary profiles. Clearly, we applied explicit methods for inlet and outlet boundary conditions. Therein, we used pressure profiles with different magnitude. The different pressure profiles produced conditions corresponding to normal pressure and hypertension in the patient-specific models. Hence, we have considered them as patient-specific boundary conditions. These BCs are injected in the 3D patient-based RCA models for the numerical simulations.

Results and discussion

The hemodynamic parameters are evaluated for different models at specific times and locations of the patient-based 3D RCA models. The difference in magnitude of WSS can be explained by the difference in the models themselves (Figure 4) and the WSS results are extensively governed by the degree of stenoses (Bit and Chattopadhay 2014b). The WSS gradient quantifies the spatial variations of hemodynamic forces on the vessel walls (Vignon-Clementel et al. 2006; Bahrami and Norouzi 2018; Park et al. 2016). The values are relatively higher in the stenosed

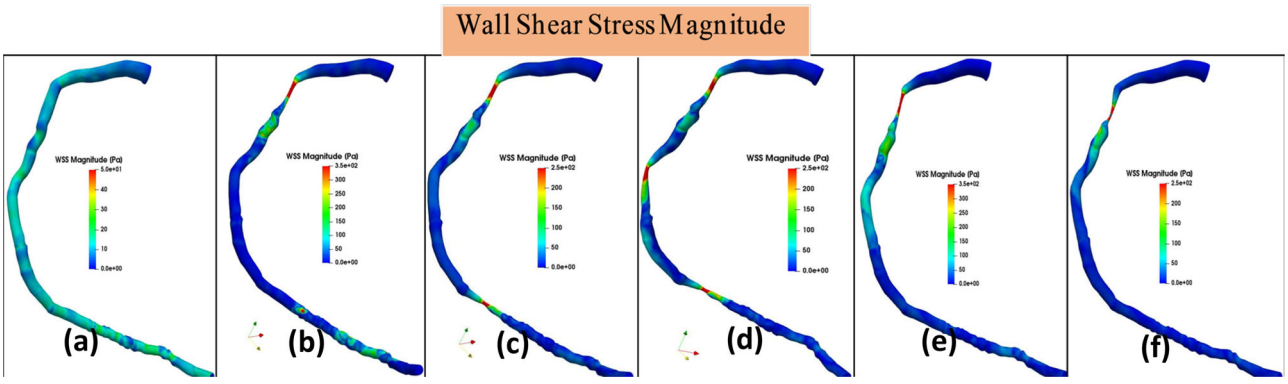

Figure 4. Comparison of the results of the WSS magnitude distribution in the healthy, single stenosis with 70%, 80%, 90% and multiple stenoses models.

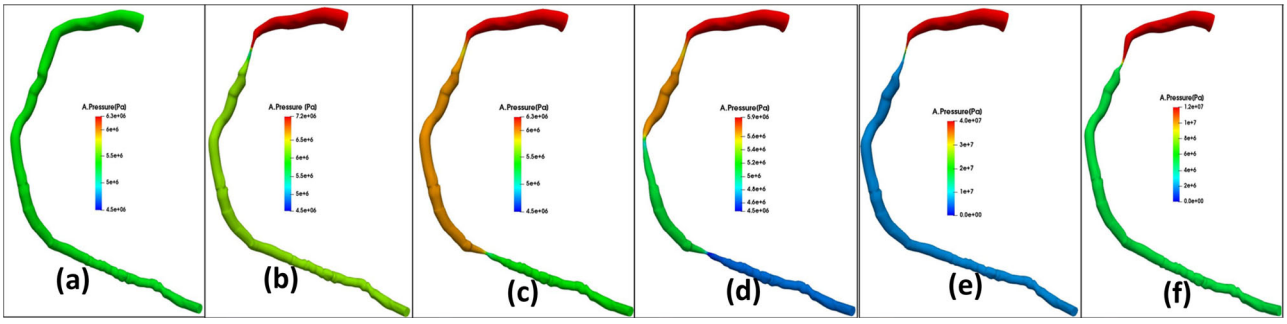

Figure 5. Numerical results comparison of the time-average pressure difference in the healthy, one, two and multiple stenoses models, respectively.

regions than in the ones without stenosis. Figure 4(a) shows the WSS magnitude distribution results in the healthy model. It is obvious that the WSS magnitude distribution values are very uniform over the vessel wall and the values are between 15 [Pa] and 25 [Pa]. On the other hand, Figure 4(b–f) represent the WSS magnitude results in the diseased models with different sizes of stenosis and in different locations of the computational domains. In Figure 4(b), the throat (stenosis) region displays a high relative WSS magnitude (more than 350 [Pa]) in one stenosis models where the upper or lower stream areas show very low magnitude values (less than 50 [Pa]). In the multiple stenoses models (Figure 4(c,d)), it is more distinguishable that the value of the relative WSS magnitude is even higher in the stenosis throat areas. Therefore, the WSS magnitude distribution results differ in the stenosis area/s compared to unstenosed regions in the RCA computational models. Figure 5 represents the mean arterial pressure difference in the different sizes of stenosis RCA models. It is obvious that the relative mean arterial pressure difference in pulsatile blood flow simulations can be explained by the difference in the models' results themselves (Figure 5). In Figure 5(a), it is illustrated that the time-average pressure difference is very uniform over the vessel and approximately 5.1e + 6 [Pa] in the healthy RCA model. Figure 5(b–f) show that the time-average pressure differences in the upstream are much higher compared to the downstream of the stenosis.

The relative pressure difference depends on the percentage of AS and multi-stenoses conditions. The highest percentage of AS model represents the highest-pressure difference in the computational domains. Figure 6 represents the numerical simulation results of velocity magnitude in the inlet position and the relative pressure difference conditions at the outlet position of the patient's RCA model. The normative and hypertensive pressure profiles are shown for the normal and hypertension blood pressure in the RCA model. The high-pressure profile produces the higher pressure in the vessel boundary condition in the RCA model. On the other hand, a normal pressure profile is recorded as lower pressure. Figure 6(b) shows that the velocity profiles condition is inversely related to the onset and exit positions. In the pulsatile flow simulation, we chose 500-time steps for both flow and pressure cases.

The single and multiple stenoses models refer to the pressure differences that are very distinguishable

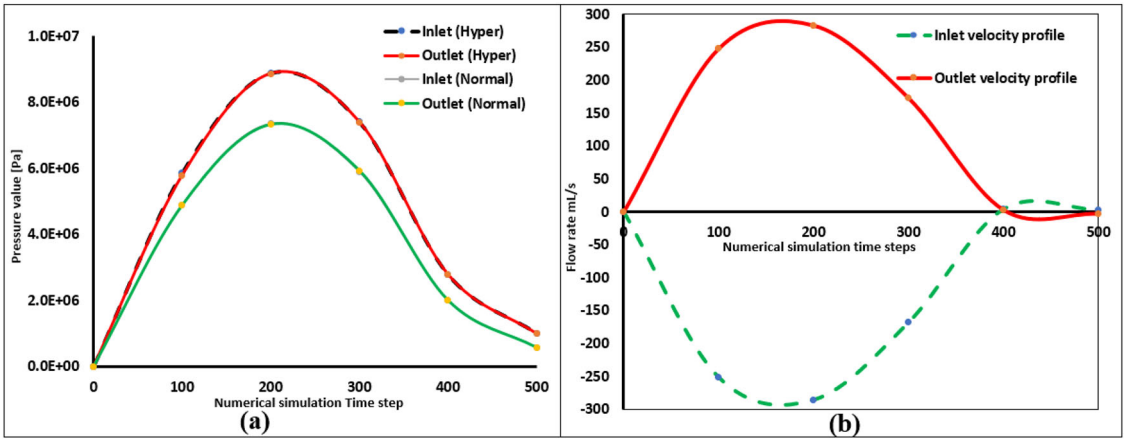

Figure 6. The simulation results of normal and hypertension mean vessel pressure conditions, velocity magnitude in healthy model.

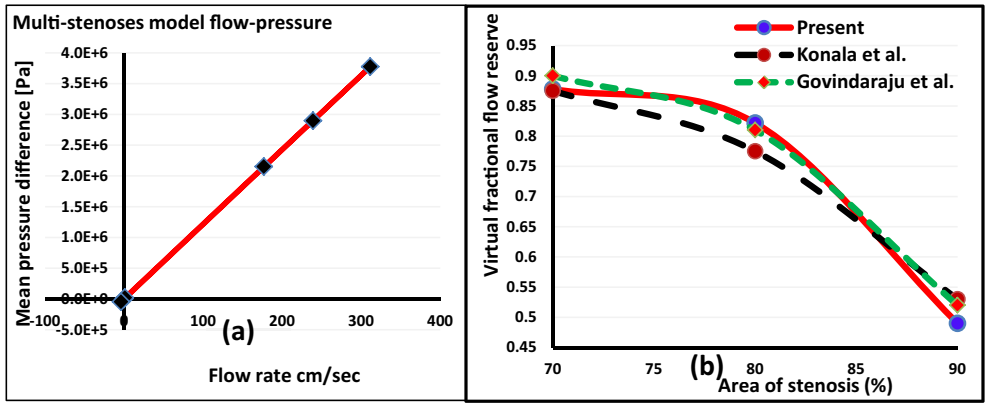

Figure 7. The simulation results of (a) linear relation of flow and pressure results in the MSS model. (b) represents the comparison results of vFFR.

between the upstream and downstream of the lesion area(s). The one stenosis model results, i.e. 70% AS model simulation, illustrate that the upstream pressure is about 7.0e + 6 [Pa] and the downstream pressure is about 6.1e + 6 [Pa] compared to the stenosed region. The MSS models, i.e. in the two and three stenoses models, recorded that the upstream pressures are about 6.4e + 6 [Pa] and about 6.0e + 6 [Pa] where as the downstream pressures are 5.3e + 6 [Pa] and 4.7e + 6 [Pa], respectively. The vFFR value of the one stenosis, two stenoses and three stenoses models are 0.871, 0.828 and 0.783, respectively, indicating that the MSS are very significant since the value of vFFR is less than the value 0.8 (Pijls et al. 2000). The 80% one stenosis model simulation results illustrate that the upstream pressure is 0.73e + 7 [Pa] and the downstream pressure is 6.0e + 6 [Pa] compared to the stenosed region and in the 90% stenoses model inscribed that the upstream pressure is 1.3e + 7 [Pa] and the downstream pressure is 6.2e + 6 [Pa]. Hence the vFFR values in 80% and 90% models are ≈0.822 and ≈0.477, respectively. Hence, the values of vFFR for 70%, 80% and 90% are significant compare with some other researcher works.

The vFFR value of the one stenosis and three stenoses models are 0.871 and 0.783, respectively, which indicates that the MSS models are very significant since the value of vFFR is less than 0.8. For numerical simulation validation, we compare the 70%, 80% and 90% area of stenosis models vFFR simulations with different research works.

Figure 7 represents the comparison of the numerical results with the published study that is included in the literature (Konala et al. 2011; Govindaraju et al. 2016). Figure 7(b) shows that the results of this study are similar to the results obtained by Konala et al. and Govindaraju et al. It is worth mentioning that these researchers used commercial 3D model software and commercial numerical codes. In the case presented herein, we only used open source techniques for simulation and analysis purposes. On the other hand, Li et al. (Kamangar et al. 2017)

demonstrated the linear relationship between flow and pressure for idealized and experimental MSS coronary artery models without branching of coronary artery. In this study, we include the 3D patient-based model simulation. This study illustrates that the flow and pressure difference in the patient-based MSS model is also linear. The result reflects that the pressure is higher for increased flow rates in the MSS model.

The results illustrate that the hypertensive pressure is higher than the normal pressure in simulations. The comparisons to results obtained using vFFR are competitive and acceptable regarding the published results. Hence, vFFR results might aid the clinical decision for coronary revascularization.

Conclusion

The aim of this study was to setup a framework to predict the functional response of coronary blood flow using a non-invasive method. The results provide the CHD interference that a physician can use for the diagnosis of coronary abnormalities in comprehensive way. The present work can be used to further the basic understanding of hemodynamic parameters and their impact on vFFR measurement techniques in order to provide insights into physiology of multiple sequential stenoses. The results are adequate for actual clinical applications but there are some limitations in the procedures such as accurate 3D model reconstruction, manually stenoses generation and capillary resistance consideration which require more studies to overcome the clinical application. We hope that this technique could be used as a non-invasive, low-risk and less expensive procedure to predict the severity of coronary lesions.

Disclosure statement

No potential conflict of interest was reported by the author(s).

References

Ahrens J, Geveci B, Law C. 2005. ParaView: an end-user tool for large-data visualization. Vis Handb. 836:717–731.

Bahrami S, Norouzi M. 2018. A numerical study on hemodynamics in the left coronary bifurcation with normal and hypertension conditions. Biomech Model Mechanobiol. 17(6):1785–1796.

Beier S, Ormiston J, Webster M, Cater J, Norris S, Medrano-Gracia P, Young A, Cowan B. 2016. Impact of bifurcation angle and other anatomical characteristics on blood flow – a computational study of non-stented and stented coronary arteries. J Biomech. 49(9):1570–1582.

Bit A, Alblawi A, Chattopadhyay H, Quais QA, Benim AC, Rahimi-Gorji M, Do H-T. 2020. Three dimensional numerical analysis of hemodynamic of stenosed artery considering realistic outlet boundary conditions. Comput Methods Programs Biomed. 185:105163.

Bit A, Chattopadhay H. 2014a. Assessment of rheological models for prediction of transport phenomena in stenosed artery. Prog Comput Fluid Dynam Int J. 14(6):363.

Bit A, Chattopadhay H. 2014b. Numerical investigations of pulsatile flow in stenosed artery. Acta Bioeng Biomech. 16(4):33–44.

Bit A, Chattopadhay H. 2018. Acute aneurysm is more critical than acute stenoses in blood vessels : a numerical investigation using stress markers. BioNanoScience. 8(1): 329–336.

Bit A, Ghagare D, Rizvanov AA, Chattopadhyay H. 2017. Assessment of influences of stenoses in right carotid artery on left carotid artery using wall stress marker. 2017:2935195.

Cademartiri F, Seitun S, Clemente A, La Grutta L, Toia P, Runza G, Midiri M, Maffei E. 2017. Myocardial blood flow quantification for evaluation of coronary artery disease by computed tomography. Cardiovasc Diagn Ther. 7(2):129–150.

Chen X, Gao Y, Lu B, Jia X, Zhong L, Kassab GS, Tan W, Huo Y. 2016. Hemodynamics in coronary arterial tree of serial stenoses. PLoS One. 11(9):1–13.

Gottsauner-Wolf M, Sochor H, Moertl D, Gwechenberger M, Stochenhuber F, Probst P. 1996. Assessing coronary stenosis. Quantitative coronary angiography versus visual estimation from cine-film or pharmacological stress perfusion images. Eur Heart J. 17(8):1167–1174.

Govindaraju K, Viswanathan GN, Badruddin IA, Kamangar S, Salman Ahmed NJ, Al-Rashed AA. 2016. The influence of artery wall curvature on the anatomical assessment of stenosis severity derived from fractional flow reserve: a computational fluid dynamics study. Comput Methods Biomech Biomed Engin. 19(14):1541–1549.

Hoque KE, Sawall S, Hoque MA, Hossain MS. 2018. Hemodynamic simulations to identify irregularities in coronary artery models. J Adv Math Comput Sci. 28(5): 1–19.

Johnston BM, Johnston PR, Corney S, Kilpatrick D. 2004. Non-Newtonian blood flow in human right coronary arteries: steady state simulations. J Biomech. 37(5): 709–720.

Ju S, Gu L. 2019. Hemodynamic interference of serial stenoses and its impact on FFR and iFR measurements. Appl Sci. 9(2):279.

Kamangar S, Badruddin IA, Govindaraju K, Nik-Ghazali N, Badarudin A, Viswanathan GN, Ahmed NJS, Khan TMY. 2017. Patient-specific 3D hemodynamics modelling of left coronary artery under hyperemic conditions. Med Biol Eng Comput. 55(8):1451–1461.

Kim HJ, Vignon-Clementel IE, Coogan JS, Figueroa CA, Jansen KE, Taylor CA. 2010. Patient-specific modeling of blood flow and pressure in human coronary arteries. Ann Biomed Eng. 38(10):3195–3209.

Konala BC, Das A, Banerjee RK. 2011. Influence of arterial wall-stenosis compliance on the coronary diagnostic parameters. J Biomech. 44(5):842–847.

Li S, Chin C, Thondapu V, Poon EKW, Monty JP, Li Y, Ooi ASH, Tu S, Barlis P. 2017. Numerical and experimental investigations of the flow–pressure relation in multiple sequential stenoses coronary artery. Int J Cardiovasc Imaging. 33(7):1083–1088.

Seo J, Schiavazzi DE, Marsden AL. 2019. Performance of preconditioned iterative linear solvers for cardiovascular simulations in rigid and deformable vessels. Comput Mech. 64(3):717–739.

Mittal R, Seo JH, Vedula V, Choi YJ, Liu H, Huang HH, Jain S, Younes L, Abraham T, George RT, et al. 2016. Computational modeling of cardiac hemodynamics: current status and future outlook. J Comput Phys. 305: 1065–1082.

Morris PD, Iqbal J, Chiastra C, Wu W, Migliavacca F, Gunn JP. 2018. Simultaneous kissing stents to treat unprotected left main stem coronary artery bifurcation disease; stent expansion, vessel injury, hemodynamics, tissue healing, restenosis, and repeat revascularization. Catheter Cardiovasc Interv. 92(6):E381–E392.

Morris PD, Ryan D, Morton AC, Lycett R, Lawford PV, Hose DR, Gunn JP. 2013. Virtual fractional flow reserve from coronary angiography: modeling the significance of coronary lesions. Results from the VIRTU-1 (VIRTUal fractional flow reserve from coronary angiography) study. JACC Cardiovasc Interv. 6(2):149–157.

Nørgaard BL, Leipsic J, Gaur S, Seneviratne S, Ko BS, Ito H, Jensen JM, Mauri L, De Bruyne B, Bezerra H, et al. 2014. Diagnostic performance of noninvasive fractional flow reserve derived from coronary computed tomography angiography in suspected coronary artery disease: the NXT trial (Analysis of coronary blood flow using CT angiography: next steps). J Am Coll Cardiol. 63(12): 1145–1155.

Park J-B, Choi G, Chun EJ, Kim HJ, Park J, Jung J-H, Lee M-H, Otake H, Doh J-H, Nam C-W, et al. 2016. Computational fluid dynamic measures of wall shear stress are related to coronary lesion characteristics. Heart. 102(20):1655–1661.

Pijls NH, De Bruyne B, Bech GJ, Liistro F, Heyndrickx GR, Bonnier HJ, Koolen JJ. 2000. Coronary pressure measurement to assess the hemodynamic significance of serial stenoses within one coronary artery: validation in humans. Circulation. 102(19):2371–2377.

Shi C, Zhang D, Cao K, Zhang T, Luo L, Liu X, Zhang H. 2017. A study of noninvasive fractional flow reserve derived from a simplified method based on coronary computed tomography angiography in suspected coronary artery disease. Biomed Eng Online. 16(1):1–15.

Takagi H, Ishikawa Y, Orii M, Ota H, Niiyama M, Tanaka R, Morino Y, Yoshioka K. 2019. Optimized interpretation of fractional flow reserve derived from computed tomography: comparison of three interpretation methods. J Cardiovasc Comput Tomogr. 13(2):134–141.

Updegrove A, Wilson NM, Merkow J, Lan H, Marsden AL, Shadden SC. 2017. SimVascular: an open source pipeline for cardiovascular simulation. Ann Biomed Eng. 45(3): 525–541.

Vignon-Clementel IE, Alberto Figueroa C, Jansen KE, Taylor CA. 2006. Outflow boundary conditions for three-dimensional finite element modeling of blood flow and pressure in arteries. Comput Methods Appl Mech Eng. 195(29-32):3776–3796.

Vinoth R, Adhikari R, Kumar D. 2016. Computational simulation of blood flow in normal and diseased artery: a review. Indian J Sci Technol. 9(15):1–15.

Waller BF. 1989. The eccentric coronary atherosclerotic plaque: morphologic observations and clinical relevance. Clin Cardiol. 12(1):14–20.

Yoshikawa Y, Nakamoto M, Nakamura M, Hoshi T, Yamamoto E. 2019. On-site evaluation of CT-based fractional flow reserve using simple boundary conditions for computational fluid dynamics. Int J Cardiovasc Imaging. 36(2):337–346.

Zuin M, Rigatelli G, Vassilev D, Ronco F, Rigatelli A, Roncon L. 2019. Computational fluid dynamic-derived wall shear stress of non-significant left main bifurcation disease may predict acute vessel thrombosis at 3-year follow-up. Heart Vessels. 35(3):297–306.